REFERENCES AND NOTES

1. For a general discussion, see J. Casti, *New Sci.* **2082**, 30 (1997).
2. L. M. Adleman, *Science* **266**, 1021 (1994).
3. R. J. Lipton, *ibid.* **268**, 542 (1995).
4. G. Paun, *J. Autom. Lang. Comb.* **1**, 27 (1996).
5. F. Guarnieri, M. Fliss, C. Bancroft, *Science* **273**, 220 (1996).
6. M. R. Garey and D. S. Johnson, *Computers and Intractability* (Freeman, New York, 1979).
7. P. D. Kaplan, Q. Ouyang, D. S. Thaler, A. Libchaber, *J. Theor. Biol.* **188**, 333 (1997), and references therein.
8. S. N. Ho, H. D. Hunt, R. M. Horton, J. K. Pullen, L. R. Pease, *Gene* **77**, 51 (1989).
9. K. Jayaraman, S. A. Fingar, J. Fyles, *Proc. Natl. Acad. Sci. U.S.A.* **88**, 4084 (1991).
10. W. P. Stemmer, A. Crameri, K. D. Ha, T. M. Brennan, H. L. Heyneker, *Gene* **164**, 49 (1995).
11. R. DeSalle, M. Barcia, C. Wray, *Experientia* **49**, 906 (1993).
12. W. P. Stemmer, *Proc. Natl. Acad. Sci. U.S.A.* **91**, 10747 (1994).
13. All PCR processes were performed on a Perkin-Elmer GeneAmp PCR system 9600 machine. For POA processing, 4 pmol of each DNA fragment and 2 units of AmpliTaq DNA polymerase, Stoffel fragment (Perkin-Elmer) in PCR buffer [10 mM tris-HCl, 50 mM KCl, 2.2 mM MgCl$_2$, 0.8 mM deoxynucleotide triphosphate (dNTP), pH 8.3, at 25°C] to a total volume of 40 μl were processed for 40 cycles (94°C for 30 s, 60°C for 30 s, and 72°C for 30 s). For general PCR, 0.2 μl of template solution, 20 pmol of primers, and 2 units of *Taq* DNA polymerase (Gibco-BRL) in PCR buffer [50 mM KCl, 10 mM tris-HCl, 2 mM MgCl$_2$, 10 mM (NH$_4$)$_2$SO$_4$, 0.8 mM dNTP, pH 8.8, at 25°C] to a volume of 40 μl were processed for 25 cycles (94°C for 30 s, 65°C for 30 s, and 72°C for 30 s).
14. The restriction enzyme digest operation was conducted following the protocol of New England Biolabs.
15. The mutagenesis process followed standard protocols (*20*): (i) We added a tail to the ends of answer DNA that is homologous (complementary) to parts of M13 phage DNA. PCR with specially designed primers was applied for this purpose. One primer consisted of 12-bp DNA homologous to M13 phage DNA (positions 6269 to 6280) and 15 bp of P_0 (GCTGGAGCTCCACGTAGAATTCTGCGA); the other primer consisted of 12-bp DNA complementary to M13 phage DNA (positions 6375 to 6386) and 15 bp of P_6 (GAATTGGGTACCCTGGATCCCGCCC). The first primer was phosphorylated at the 5′ end with T4 polynucleotide kinase (New England Biolabs). (ii) The dsDNA of the PCR solution in step (i) was digested by λ exonuclease (Gibco-BRL) following the supplier's instructions. The DNA strand that contains a 5′ phosphate was thus digested. (iii) Mutagenetic M13 phage DNA (containing answer DNA) was synthesized using the ssDNA from step (ii) as primer and wild-type M13 phage DNA as template.
16. Transfection, phage purification, and DNA extraction were conducted following standard protocols (*20*). The DNA sequencing was done by the Rockefeller University Protein/DNA Technology Center.
17. The DNA in the data pool was purified by ethanol precipitation. The ssDNA was digested in S1 nuclease buffer (50 mM NaAc, 280 mM NaCl, and 4.5 mM ZnSO$_4$) with 2 units of S1 nuclease at room temperature for 2 min.
18. K. A. Eckert and T. A. Kunkel, *PCR Methods Appl.* **1**, 17 (1991).
19. M. Chee *et al.*, *Science* **274**, 610 (1996).
20. J. Sambrook, E. F. Fritsch, T. Maniatis, *Molecular Cloning* (Cold Spring Harbor Laboratory Press, Cold Spring Harbor, NY, 1987).
21. We thank D. Boneh, who proposed the maximal clique problem and the binary number–based algorithm for solving it, and D. Thaler, who suggested the use of POA to build the data pool.

23 June 1997; accepted 3 September 1997

Direct Visualization of Individual Cylindrical and Spherical Supramolecular Dendrimers

S. D. Hudson,* H.-T. Jung, V. Percec,* W.-D. Cho, G. Johansson, G. Ungar,* V. S. K. Balagurusamy

Electron microscopy methods have been used to visualize individual spherical and cylindrical supramolecular dendrimers, providing definitive confirmation of the structures suggested by previous x-ray diffraction analysis that assumed a microsegregated model. These dendrimers are self-assembled, self-organized, and aligned spontaneously and simultaneously in hexagonal columnar or cubic thermotropic liquid-crystal phases with high uniformity. Homeotropic and planar ordering of the hexagonal columnar liquid crystal was precisely controlled by a variety of surfaces. The stiffness of these cylinders was evaluated by examining their planar texture and its defects.

Control of the order of molecular, macromolecular, and supramolecular synthetic organic materials is an important goal in chemistry, that can be used to improve the materials' properties (*1–3*). Building blocks based on dendritic architectures (*4*), which have a hierarchy of branched structures, can generate molecular objects of nanoscale dimensions (*5*, *6*), and self-assembly of supramolecular dendrimers from monodendritic building blocks can provide rapid access to the construction of giant architectures (*7*). The elucidation of the shape of dendrimers in solution and in the bulk represents one of the most important prerequisites for access to their controlled design (*4–6*). A transition from an ovoidal to a spherical shape by increasing the generation number has been predicted for dendrimers (*8*). Various studies have suggested that in solid and melt states, dendrimers or their aggregates, or both, can adopt either spherical (*5*) or rod-like shapes (*6*). However, because the previously studied dendritic systems lacked long-range positional order, individual objects could not be isolated, and therefore, the shape and size of these dendrimers could not be determined.

Recently, we have advanced a rational design and synthesized monodendrons that self-assemble through various molecular recognition mechanisms into rod-like (*9*), cylindrical (*10*), and spherical (*11*) supramolecular dendrimers. The cylindrical supramolecular dendrimers self-organize into a thermotropic hexagonal columnar (Φ_h) (*10*) [two-dimensional (2D) p6mm lattice], whereas the spherical ones form a novel thermotropic cubic (Cub) liquid-crystalline (LC) phase of Pm$\bar{3}$n symmetry (3D lattice) (*11*). The lattices of both supramolecular LC assemblies can be oriented by using techniques available for the alignment of molecular LC assemblies (*12*) to generate single-domain LCs. Analysis of mono- and polydomain LCs by x-ray diffraction (XRD) allowed the determination of the shape, size, and structure of supramolecular dendrimers organized in a lattice (*9–11*). However, owing to the ubiquitous phase problem, uncertainty is always present in crystallographic analyses based on limited numbers of reflections observed in LC systems (up to 13 different reflections obtained for **3**) (*11*). In our XRD experiments (*11*), the key assumption was that aromatic and aliphatic moieties segregate, aliphatic regions having uniform density. Thus, direct visualization of the structure by transmission electron microscopy (TEM) is invaluable in testing the assumptions on which the XRD structure is based (*13*). We directly imaged individual species of cylin-

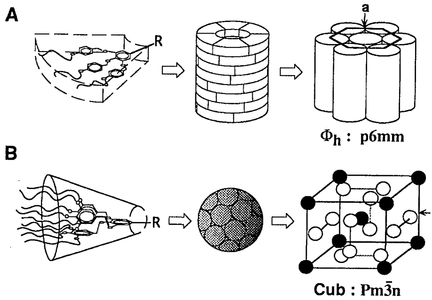

Fig. 1. Self-assembly of (**A**) first-generation flat tapered monodendrons into a supramolecular cylindrical dendrimer and the subsequent formation of the p6mm Φ_h LC supramolecular assembly, and (**B**) of second-generation conical monodendrons into a spherical dendrimer and the subsequent formation of the Pm$\bar{3}$n Cub LC supramolecular assembly [modified version reprinted with permission from Balagurusamy *et al.* (*11*), copyright 1997 by American Chemical Society].

S. D. Hudson, H.-T. Jung, V. Percec, W.-D. Cho, G. Johansson, The W. M. Keck Laboratories for Organic Synthesis, Department of Macromolecular Science, Case Western Reserve University, Cleveland, OH 44106–7202, USA.
G. Ungar and V. S. K. Balagurusamy, Department of Engineering Materials and Centre for Molecular Materials, The University of Sheffield, Sheffield S1 3JD, UK.

*To whom correspondence should be addressed.

drical and spherical supramolecular dendrimers arranged into p6mm Φ_h and Pm$\bar{3}$n Cub LC lattices, respectively. The orientation of these lattices was manipulated by various surfaces to produce large domains with a high degree of order. The analysis of their defects allowed the determination of the relative stiffness of these supramolecular columns.

Figure 1 outlines the mechanisms by which flat tapered and conical monodendrons generate, respectively, cylindrical and spherical supramolecular dendrimers (*10, 11*). Subsequent self-organization is also shown. Two monodendrons, **1** and **2**, which self-assemble into cylindrical supramolecular dendrimers (*10*), and two others, **3** and **4** (*11*), which self-assemble into spherical supramolecular dendrimers, were studied (Fig. 2) (*14*).

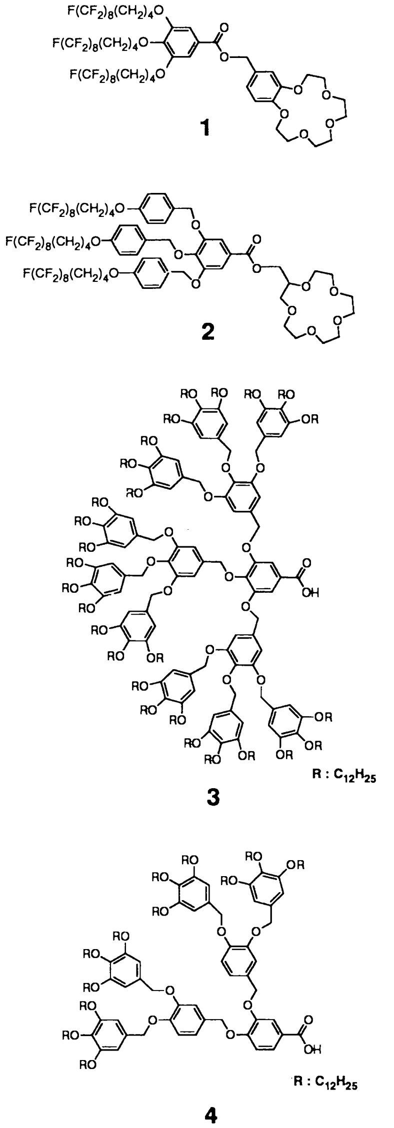

Fig. 2. Tapered **1** and **2** and conical **3** and **4** monodendrons analyzed by TEM.

The Φ_h phase of **1** and **2** was oriented by surface anchoring in thin films (*15*). Excellent planar alignment of the supramolecular columns was achieved on polar substrates such as water and glycerin. Homeotropic alignment was produced on untreated glass and carbon films. Metal substrates such as polycrystalline Pd produce alignments that depend on their crystallographic orientation. Homeotropically aligned structures (with thickness of up to millimeter size) can be transformed into planar-aligned ones by shearing. Previously, only homeotropic alignment was observed by optical microscopy (*10*). In many respects, the control of the orientation of these supramolecular cylindrical LC assemblies by surface anchoring resembles that for various molecular assemblies such as LCs (*16*), crystals (*17*), and to a lesser extent, monolayers and Langmuir-Blodgett films (*18*). The LC nature of these supramolecular materials ensures thermodynamic control of the ordering process. Therefore, self-assembly, self-organization, and alignment of these complex functional supramolecular systems take place spontaneously and simultaneously. Previous examples of surface-aligned supramolecular assemblies were limited to less-complex systems such as lyotropic surfactants (*19*) and block copolymers, which also exhibit a slower rate of self-organization (*20*).

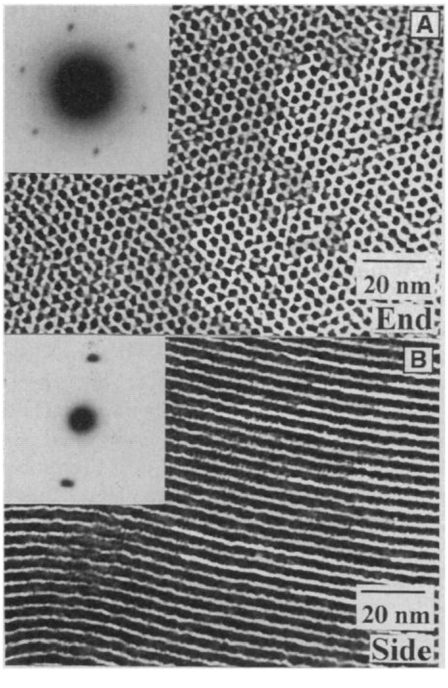

Fig. 3. Phase-contrast micrograph of (**A**) homeotropically and (**B**) planar-aligned Φ_h LC assemblies generated by supramolecular cylinders self-assembled from **1**. (Insets) ED patterns. The image represents a projection through a film having a thickness equal to approximately 15 column diameters (diameter is 49 Å). On the original negatives, (10), (2$\bar{1}$), (20), (3$\bar{1}$), and (30) reflections are seen for homeotropic specimens, examined with the incident beam parallel to the cylinder axis. For planar specimens, (10) and (20) reflections are observed at normal incidence. The (2$\bar{1}$) reflection becomes visible when the sample is tilted 30° about the cylinder axis (*30*).

The TEM micrographs of aligned **1** (lattice constant *a* = 45.7 Å from XRD at 70°C) (*10*) present end and side views of the Φ_h LC assemblies (Fig. 3). The cores of the supramolecular columns are dark (Fig. 3A), indicating the regions of higher density (in unstained samples) and the place where RuO_4 was preferentially complexed (in stained samples). Because this agent stains the aromatic and the crown-ether fragments of the monodendrons, the TEMs reconfirm previous XRD analysis (*10*) that suggests crown-ethers form the core of the column (Fig. 1) and demonstrate that there is a high degree of perfection in the packing of these infinitely long columns. Compound **2** (*a* = 45.6 Å by XRD at 100°C) self-assembles into much stiffer columns than **1** (*a* = 45.7 Å by XRD at 70°C) when quenched from 50° to 20°C (Fig. 4). The relative stiffness of columns **1** and **2** in the LC phase was evaluated from their distortion near a dislocation defect (Fig. 4) (*21*). The columns adjacent to the dislocation are tilted slightly with respect to the central column. The permeation length λ is proportional to the square of the length *L* of the bent segment of a column divided by its distance *z* from the central columns, that is $\lambda \cong L^2/z$, and therefore, estimates the column stiffness (*22*). This value was predicted to be of the order of column diameter (*a*) (*23*). In the case of **1**, λ is 16 Å (in rescaled form, λ = 0.35 ± 0.15*a*) and in the case of **2**, λ is 230 Å (that is, 5 ± 1*a*). Because of the large diameters of **1** and **2**, their λ values are larger than the only literature data available for a rigid rod polymer, λ = 8 Å = 0.9*a* (*24*). In addition, the rescaled

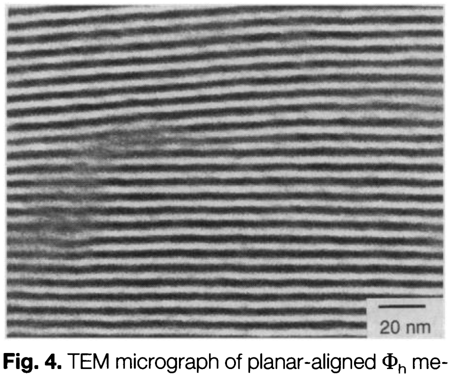

Fig. 4. TEM micrograph of planar-aligned Φ_h mesophase of **2**, quenched to 20°C from 50°C. A dislocation is observed approximately 11 columns down from the top of the figure. The column diameter is 58 Å.

value λ of **2** is significantly larger than 1.0. This is consistent with a column based on a rigid core surrounded by a deformable sheath. These data indicate that the rigidity of these supramolecular columns and their interactions can each be controlled independently by design.

XRD analysis of the cubic phases of compounds **3** and **4** determined their space groups to be Pm$\bar{3}$n (*11*). On the basis of the assumption that the aliphatic and aromatic portions of the molecules are segregated, two possible structures were derived from Fourier synthesis (*11*). The structure that produced the greatest degree of segregation of these segments is a spherical model (Figs. 1B and 5E). The closest rival structure to the spherical model is a cubic phase consisting of three sets of mutually perpendicular columns (Fig. 5G). TEM imaging of **3** and **4** provides complementary, direct, and conclusive discrimination of these two models.

A TEM image of the spherical supramolecular dendrimer self-assembled from 16 **4** monodendrons (*11*) is shown in Fig. 5A. Before this report, a related Pm$\bar{3}$n Cub lattice was observed by a combination of XRD and freeze-fracture TEM only in a lyotropic phase of biological lipids (*25*). Recently, this phase was predicted theoretically for short diblock copolymers in the presence of a diluent (*26*). Our visualization was made possible by the preparation of large, single-crystal LC and by the adequate beam resistance of these materials. Electron diffraction (ED) of this sample is consistent with XRD (a = 87.3 Å at 58°C) (*11*, *27*).

Six low-angle reflections, which are consistent with XRD, were detected by ED (*27*). They are also present in the power spectrum (Fig. 5D) calculated from the TEM image (Fig. 5A), and because their phases are preserved in the TEM image, the structure can be determined directly by comparison of the image with projections from the two rival models (Fig. 5, E and F and G and H). The [001] projection of each contains two sets of perpendicular dark lines. At their intersection, the columnar model produced a dark spot (Fig. 5H), whereas the spherical model produced a white one (Fig. 5F). Although the lightened corner can be seen directly on the original image (Fig. 5A), it becomes more clear through the use of Fourier filtering, an averaging technique (Fig. 5B). The Fourier transform is filtered by setting the transform to zero everywhere except in the neighborhood of these diffraction peaks. If the neighborhood is chosen to be narrow, then the averaging is extensive, whereas if the neighborhood is chosen to be larger, the average is more local and noise is selectively introduced (*28*). The three most intense peaks of the transform were selected, and a neighborhood centered on each, having a diameter of 0.003 Å^{-1}, was used. The extent of averaging is therefore approximately 4 unit cells by 4 unit cells. The bright spot at the intersection of the dark lines can now be observed easily (Fig. 5B). This provides definitive confirmation for the spherical model (Figs. 1B and 5, A and B) (*11*). The most common defects observed in the Cub phase of **4** are partial dislocations and grain boundaries comprising arrays of such dislocations. These defects are also consistent with the spherical model.

Having determined by TEM the correct phases for the principal Fourier components, the 3D distribution of the electron density was calculated from XRD intensities (Fig. 6). The surfaces represented in Fig. 6 envelope spherical regions of the highest density, which make up 19% of the total volume—that is, the part that is expected to be occupied by the aromatic dendritic cores. The rest of the volume contains aliphatic chains of relatively uniform density (*11*). Whereas the supramolecular dendrimers at the corners and at the body center are spherical, those on the face bisectors are slightly tetrahedrally distorted, according to the symmetry of the cavity in which they reside (*11*).

The most notable features of the monodendritic building blocks investigated here are their structural simplicity (Fig. 1); ability to self-assemble largely under thermodynamic control, through the combination of shape complementarity and demixing of aliphatic and aromatic segments as an organizing force; and their unexpectedly high capability to align on surfaces. This mechanism of self-assembly contrasts that of previous supramolecular dendrimers, which is dominated by attractive specific interactions (*7*) and resembles both in simplicity and efficiency the assembly of biological systems (*29*). The ability of these cylindrical dendrimers to align by extremely simple and convenient techniques combined with their controlled stiffness and their well es-

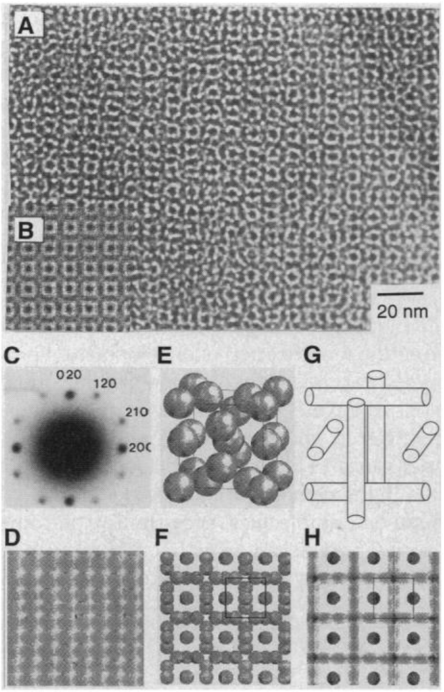

Fig. 5. TEM and ED of the Pm$\bar{3}$n Cub LC phase of the supramolecular dendrimer of **4**. Shown are (**A**) the raw image; (**B**) a reconstructed image, based on Fourier filtering of the (200), (210), and (400) peaks contained in the power spectrum (D); (**C**) the corresponding ED pattern; (**D**) the Fourier transform power spectrum of the raw image; (**E**) schematic model of the phase generated from supramolecular spherical dendrimers; (**F**) [001] projection of the spherical model; (**G**) rival schematic model of the phase generated from supramolecular columnar dendrimers; and (**H**) [001] projection of the rival cylindrical model. The boxed regions in (F) and (H) correspond to one unit cell as illustrated in (E) and (G), respectively. The power spectrum [that is, the Fourier transform multiplied by its complex conjugate (D)] obtained from (A) reproduces the ED pattern (C). Each of the six reflections of the [001] zone seen by ED (*27*) are present in (D), yet because the defocus was selected for high resolution, the relative intensity of the (400) reflection, for example, is enhanced. The (100) and (300) reflections are absent, as expected. Also absent is the (110) reflection which, though an allowed reflection for the Pm$\bar{3}$n space group, was only very weakly detected by XRD (*11*). From analysis of the diffuse background of (D), the resolution of the image (A) was calculated to be 20 Å, and the circular symmetry of the background (D) indicated no astigmatism.

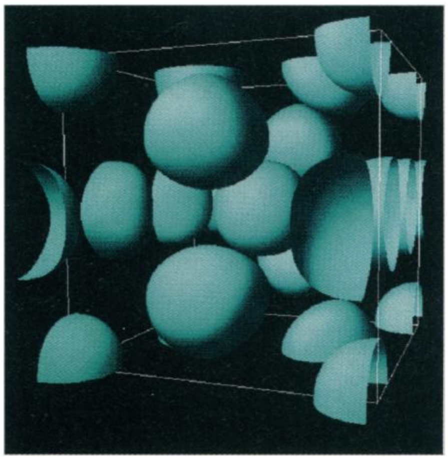

Fig. 6. The 3D electron density distribution of the Pm$\bar{3}$n Cub phase (a = 79.2 Å at 80°C) of the spherical supramolecular dendrimers self-assembled from 16 **3** monodendrons. These isoelectron surfaces were generated from XRD by Fourier synthesis with the structure factor phases determined by TEM.

tablished capability to be functionalized via covalent and noncovalent bonding (*4–6*, *9*, *10*) opens new strategies for design at the molecular level in areas such as functional membranes and devices based on ionic, electronic, photonic, and control release.

REFERENCES AND NOTES

1. P.-G. de Gennes, *Angew. Chem. Int. Ed. Engl.* **31**, 842 (1992).
2. A. Gaveffotti, *Acc. Chem. Res.* **27**, 309 (1994); J. M. Lehn, *Supramolecular Chemistry* (VCH, Weinheim, Germany, 1995); P. Ball, *Designing the Molecular World* (Princeton Univ. Press, Princeton, NJ, 1994); M. T. Krejchi *et al.*, *Science* **265**, 1427 (1994).
3. A. Keller and G. Goldbeck-Wood, in *Comprehensive Polymer Science*, supplement 2, G. Allen, Ed. (Pergamon, Oxford, 1996), p. 241.
4. N. Ardoin and D. Astruc, *Bull. Soc. Chim. Fr.* **132**, 875 (1995); G. R. Newkome, C. N. Moorefield, F. Vögtle, *Dendritic Molecules* (VCH, Weinheim, Germany, 1996); J. M. J. Fréchet and C. J. Hawker, in (*3*), p. 71.
5. D. A. Tomalia, D. M. Hedstrand, L. R. Wilson, in *Encyclopedia of Polymer Science and Engineering*, Index Volume, H. F. Mark, N. M. Bikales, C. G. Overberger, G. Menges, Eds. (Wiley, New York, ed. 2, 1990), p. 46; J. M. J. Fréchet, *Science* **263**, 1710 (1994); G. R. Newkome *et al.*, *J. Am. Chem. Soc.* **108**, 849 (1986); W. T. S. Huck, B. H. M. Snellink-Ruël, J. W. Th. Lichtenbelt, F. C. J. M. van Veggel, D. N. Reinhoudt, *Chem. Commun.* **1997**, 9 (1997), and references cited therein; P. M. Saville *et al.*, *J. Phys. Chem.* **99**, 8283 (1995); S. S. Sheiko *et al.*, *Macromol. Rapid Commun.* **17**, 283 (1996); I. Gitsov and J. M. J. Fréchet, *J. Am. Chem. Soc.* **118**, 3785 (1996); K. L. Wooley, C. A. Klug, K. Tasaki, J. Schaefer, *ibid.* **119**, 53 (1997).
6. D. A. Tomalia and H. D. Durst, *Top. Curr. Chem.* **165**, 193 (1993); G. R. Newkome *et al.*, *Angew. Chem. Int. Ed. Engl.* **31**, 917 (1992); J. C. M. van Hest, D. A. P. Delnoye, M. W. P. L. Baars, M. H. P. van Genderen, E. W. Meijer, *Science* **268**, 1592 (1995).
7. J. M. Lehn, *Makromol. Chem. Macromol. Symp.* **69**, 1 (1993); E. C. Constable, P. Harverson, M. Oberholzer, *Chem. Commun.* **1996**, 1821 (1996); S. C. Zimmerman, F. Zeng, D. E. C. Reichert, S. V. Kolotuchin, *Science* **271**, 1095 (1996).
8. P.-G. de Gennes and H. Hervet, *J. Phys. Lett.* **44**, L351 (1983); A. M. Naylor, W. A. Goddard III, G. E. Kiefer, D. A. Tomalia, *J. Am. Chem. Soc.* **111**, 2339 (1989).
9. V. Percec, P. Chu, G. Ungar, J. Zhou, *J. Am. Chem. Soc.* **117**, 11441 (1995).
10. V. Percec, G. Johansson, G. Ungar, J. Zhou, *ibid.* **118**, 9855 (1996), and references cited therein.
11. V. S. K. Balagurusamy, G. Ungar, V. Percec, G. Johansson, *ibid.* **119**, 1539 (1997); V. Percec, W.-D. Cho, G. Ungar, V. S. K. Balagurusamy, in preparation.
12. H. Finkelmann, in *Thermotropic Liquid Crystals*, G. W. Gray, Ed. (Wiley, New York, 1987), p. 145; P.-G. de Gennes and J. Prost, *The Physics of Liquid Crystals* (Oxford Scientific, Oxford, 1993); V. Percec, in *Handbook of Liquid Crystal Research*, P. J. Collings and J. S. Patel, Eds. (Oxford Univ. Press, Oxford, 1997), p. 259.
13. E. L. Thomas. D. M. Anderson, C. S. Henkee, D. Hoffman, *Nature* **334**, 598 (1983).
14. Phase transitions in °C and corresponding enthalpy changes in kcal/mol between parentheses are: **1**, k 68 (5.26) Φ_h 78 (0.31) i, i 74 (0.25) Φ_h 0 g; **2**, k 56 (6.19) Φ_h 135 (0.82) i, i 132 (0.83) Φ_h 30 (4.27) k; **3**, k -15 (31.5) Cub 140 (1.63) i, i 127 (1.17) Cub -17 (31.0) k; **4**, k 58 (31.83) Cub 108 (0.41) i, i 99 (0.11) Cub 93 (0.03) k -23 (7.15) k.
15. Planar aligned columnar thin films were obtained by casting a 0.5 wt% toluene solution onto distilled water at a temperature where the monodendron is self-assembled into a supramolecular cylindrical dendrimer. These films were retrieved on copper grids and examined by TEM. Samples of homeotropically aligned supramolecular columnar dendrimers were obtained by annealing thin films supported on carbon. Thin films cast on water were placed on copper grids, coated with carbon, heated to the isotropic phase, and cooled (at 5°C per minute to a particular temperature, before final quenching to 20°C). Films were examined before and after staining with RuO_4 (vapors generated in a closed vessel containing a 0.5 wt% aqueous solution of RuO_4). Brightfield TEM images were obtained with a JEOL 100CX TEM, operated at 100 kV. Thin films of the spherical supramolecular dendrimers were prepared on the same support by cooling at a rate of 0.1°C per minute from 5°C above to 25°C below the isotropization temperature [i in (*14*)].
16. D. M. Walba, F. Stevens, N. A. Clark, D. C. Parks, *Acc. Chem. Res.* **29**, 591 (1996).
17. B. Lotz, *Philos. Trans. R. Soc. London Ser. A* **348**, 19 (1994).
18. L. A. Bumm *et al.*, *Science* **271**, 1705 (1996).
19. P. Oswald and M. Allain, *J. Phys. (Paris)* **46**, 831 (1985).
20. B. Collin, D. Chatenay, G. Coulon, D. Ausserre, Y. Gallot, *Macromolecules* **25**, 1621 (1992); L. H. Radzilowski, B. L. Carvahlo, E. L. Thomas, *J. Polym. Sci. Part B Polym. Phys.* **34**, 3081 (1996); P. Mansky, Y. Liu, E. Huang, T. P. Russell, C. Hawker, *Science* **275**, 1458 (1997); S. I. Stupp *et al.*, *ibid.* **276**, 384 (1997).
21. M. Kleman, in *Points, Lines and Walls* (Wiley, New York, 1983), p. 141.
22. The inclination θ of neighboring columns was measured as a function of z, the distance from the dislocation along the Burger's vector (that is, perpendicular to the central column), and λ was determined most accurately by fitting the equation

$$\theta = \frac{1}{4\sqrt{\pi}}\frac{a}{\sqrt{\lambda z}}$$

23. P.-G. de Gennes and J. Prost, in *The Physics of Liquid Crystals* (Oxford Scientific, Oxford, 1993), pp. 352, 356, and 357.
24. P. M. Wilson and D. C. Martin, *Macromolecules* **29**, 829 (1996).
25. V. Luzzatti, R. Vargas, P. Mariani, *J. Mol. Biol.* **229**, 540 (1993).
26. R. G. Larson, *Chem. Eng. Sci.* **49**, 2833 (1994).
27. The [001] zone axis is typically perpendicular to the film surface, and the ED pattern shown in Fig. 5C [containing the (200) and (210) reflections] was obtained at normal beam incidence. In addition, the following low-angle reflections in the [001] zone were observed: (400), (320), (220) and (310), listed in order of decreasing intensity. At wide angles, a diffuse ring was observed centered at 4.6 Å, indicating that the structure at the atomic level is disordered. The (211) reflection, which is strong and of comparable intensity to the (200) and (210) reflections, can be observed as expected, if the specimen is tilted 27° or 45° about the [100] axis.
28. P. Pradere, J. F. Revol, L. Nguyen, R. S. Manley, *Ultramicroscopy* **25**, 69 (1988).
29. C. Tanford, *Science* **200**, 1012 (1978).
30. ED patterns of unstained samples confirm that only negligible change in the symmetry and dimension of the supramolecular dendrimers and of their LC assemblies results from RuO_4 staining. Identical ED patterns are obtained from unstained samples. However, the material is sensitive to the electron beam, and the low-angle reflections disappear during irradiation, because the electron beam induces structural rearrangements which destroy the order. Stained samples are more resistant to the electron beam.

31. Supported by NSF and the Engineering and Physical Science Research Council, UK.

12 May 1997; accepted 21 August 1997

The Homeotic Gene *lin-39* and the Evolution of Nematode Epidermal Cell Fates

Andreas Eizinger and Ralf J. Sommer*

The fate of ventral epidermal cells differs among nematode species. Nonvulval cells fuse with the epidermis in *Caenorhabditis elegans*, whereas the homologous cells undergo apoptosis in *Pristionchus pacificus*. The homeotic gene *lin-39* is involved in the regulation of these epidermal cell fates. In *Caenorhabditis*, *lin-39* prevents cell fusion of potential vulval cells and specifies the vulva equivalence group. *Pristionchus* vulvaless mutants that displayed apoptosis of the vulval precursor cells were isolated, and point mutations in *lin-39* were identified. Thus, the evolution of these epidermal cell fates is driven by different intrinsic properties of homologous cells.

Evolutionary changes in morphology result from the modification of developmental processes. To study evolutionary transformations in development, it is essential to trace changes in the activity of individual cells and genes. The invariant development of free-living nematodes combined with the genetic and molecular accessibility of some species provide an experimental system in which to study functional alterations in homologous cells and genes during the course of evolution. We analyzed an evolutionary alteration of the fate of homologous ventral epidermal cells among members of two different nematode families.

In the ventral epidermis of *Caenorhabditis elegans*, 12 precursor cells [P1.p through P12.p; denoted as P(1–12).p] adopt either nonvulval or distinct vulval cell fates in a position-specific manner (Fig. 1, A and B) (*1*). The central cells [P(3–8).p], form a so-called vulva equivalence group because all cells have the potential to adopt vulval fates. In the third larval stage (L3), these cells adopt one of three different cell fates.

Max-Planck Institut für Entwicklungsbiologie, Abteilung Zellbiologie, Spemannstrasse 35, 72076 Tübingen, Germany.

*To whom correspondence should be addressed. E-mail: sora@mailer1.mpib-tuebingen.mpg.de